



# Sensitivity of the nocturnal and polar boundary layer to transient phenomena

Amandine Kaiser<sup>1</sup>, Nikki Vercauteren<sup>1,2</sup>, and Sebastian Krumscheid<sup>3</sup>

<sup>1</sup>Department of Geosciences, University of Oslo, Oslo, Norway

<sup>2</sup>Institut für Geophysik und Meteorologie, Universität zu Köln, Cologne, Germany

<sup>3</sup>Karlsruhe Institute of Technology, Karlsruhe, Germany

**Correspondence:** Amandine Kaiser ([amandine.kaiser@geo.uio.no](mailto:amandine.kaiser@geo.uio.no))

**Abstract.** Numerical weather prediction and climate models encounter challenges in accurately representing flow regimes in the stably stratified atmospheric boundary layer and the transitions between them, leading to an inadequate depiction of regime occupation statistics. As a consequence, existing models exhibit significant biases in near-surface temperatures at high latitudes. To explore inherent uncertainties in modeling regime transitions, the response of the near-surface temperature inversion to transient small-scale phenomena is analyzed based on a stochastic modeling approach. A sensitivity analysis is conducted by augmenting a conceptual model for near-surface temperature inversions with randomizations that account for different types of model uncertainty. The stochastic conceptual model serves as a tool to systematically investigate what types of unsteady flow features, and in what contexts, may trigger abrupt transitions in the mean boundary layer state. The findings show that the incorporation of enhanced mixing, a common practice in numerical weather prediction models, blurs the two regime characteristic of the stably stratified atmospheric boundary layer. Simulating intermittent turbulence is shown to provide a potential workaround for this issue. Including key uncertainty in models could lead to a better statistical representation of the regimes in long-term climate simulation. This would help to improve our understanding and the forecasting of climate change especially in high-latitude regions.

## 15 1 Introduction

The polar and nocturnal stably stratified boundary layer (SBL) is typically classified into two distinct regimes: a weakly (wSBL) and a very stable (vSBL) one. The wSBL is characterized by a well-defined boundary layer with relatively continuous turbulence in both space and time and it typically occurs with either cloud cover or moderate to strong winds (Mahrt, 2014). On the other hand, the vSBL is defined by strong stratification and weak winds. A sharp transition is found between those two regimes, occurring on a narrow range of wind speeds. The existence of the two distinct regimes has been shown in many studies ranging from observational studies (Mahrt, 1998; Vignon et al., 2017) to conceptual modeling (McNider, 1995; van de Wiel et al., 2017) and turbulence resolving numerical simulations (Ansorge and Mellado, 2014; Donda et al., 2015).



Conceptual models have been used to understand regime transitions and explore the relevant feedback processes which can explain the existence of the two regimes. Using a two-layer numerical model that represents the exchanges between the surface and the SBL, McNider (1995) demonstrated the presence of bistable equilibria within the system. Specifically, they showed that both wSBL and vSBL could be possible solutions for a given forcing of the SBL. Consequently, the system has the capability to undergo transitions between the two regimes due to the effects of random perturbations of the equilibrium state. As another example, the conceptual model suggested by van de Wiel et al. (2017) uses a surface energy balance model combined with a bulk parameterization of the turbulent heat transport and a simple parameterization of the soil and radiative transfer to explore the nonlinear feedback process related to the energy fluxes coupling at the land-atmosphere interface. The system as represented in the conceptual model leads to a bistable system, i.e. for example for the same wind forcing both the vSBL and wSBL are possible solutions. The authors showed that the system is bistable for a range of different parameters. Moreover, they found that the scatter seen in the bistable region of observational data can be explained by the fact that perturbations away from the equilibrium are only weakly dampened. In our study, we investigate when these perturbations lead to a numerical feedback that induces a regime transition. The existence of multi-valued solutions has strong implications on the predictability of the SBL, since small perturbations or uncertainty in initial and forcing conditions may lead to very different outcomes of the mean state of the SBL. In particular, for NWP the forecast uncertainty is significantly impacted by the spread of possible outcomes related to the before mentioned bistability. In addition, for Earth system models it is of high relevance to have a correct statistical representation of the two regimes to accurately model seasonal heat fluxes between the surface and the atmosphere.

Several observational studies have shown the abrupt character of transitions between the two stable states (Baas et al., 2019; Vignon et al., 2017). These transitions can be controlled by changes in the large-scale forcing. Based on observational data, Acevedo et al. (2019) connected regime transitions from vSBL to wSBL with a change of wind direction from first the ocean and then land. They postulated that the transition is related to a change of horizontal advection patterns. Moreover, Abraham and Monahan (2019) showed, by applying a Hidden Markov model to cluster observational data from multiple locations into two regimes, that transitions from wSBL to vSBL most likely occur shortly after sunset, hence relating them to the onset of nocturnal radiative cooling. The statistical study highlighted no regularity for vSBL to wSBL transitions, which points to possibly small-scale random features at the origin of transitions. Indeed, transient phenomena can in some cases be sufficient to induce a large-scale change in the SBL. Our hypothesis is that transitions can be due to noise-induced tipping, for example following the influence of an isolated turbulent burst that can trigger a nonlinear feedback process where turbulence is eventually regenerated in the entire boundary layer. Direct numerical simulations have shown that after a localized, random perturbation of the flow, transitions from vSBL to wSBL states can occur (Donda et al., 2015). Field studies have also revealed examples of transitions triggered by small-scale perturbations (Sun et al., 2012; Lan et al., 2022). The following numerical study analyses the sensitivity of the SBL to small-scale variability in the forcing and turbulent fluxes.

To analyze which small-scale perturbations can non-linearly amplify and lead to regime transitions, a sensitivity study is designed based on a stochastic extension of the conceptual model by van de Wiel et al. (2017). In a bistable system, abrupt transitions or tipping points can be noise-induced, meaning that a transient perturbation can be enough to trigger a regime



transition (Ashwin et al., 2012). These noise-induced transitions occur without passing a critical value of the control bifurcation parameter, here the wind velocity. Different types of noise are added to the model to represent transient phenomena. With this randomized model, we study the sensitivity of regime transitions to perturbations of the temperature dynamics and wind speed. Kaiser et al. (2020) successfully tested a statistical indicator for the dynamical stability with a similarly randomized version of the model by van de Wiel et al. (2017). Moreover, Abraham et al. (2019) developed a stochastic model with stratification-dependent transition probabilities and Ramsey and Monahan (2022) defined a data-driven stochastic differential equation model for temperature inversion variability.

60 Among the small-scale phenomena that have been shown to be relevant for regime transitions, turbulence is described by a model closure. This model structure typically relies on Monin Obhukov Similarity Theory (MOST) which assumes stationarity of the turbulent statistics and hence does not represent intermittency and turbulent bursts (Foken, 2006). This assumption is known not to hold in the vSBL (Liang et al., 2014; Mahrt and Bou-Zeid, 2020). In MOST, the closure makes use of a stability function that scales the mixing lengthscale, adjusting the amount of turbulent mixing to the dimensionless static stability of the flow (Cuxart et al., 2005). Numerical weather prediction models (NWP) use different types of stability functions, and several works have shown that the choice impacts the representation of SBL regimes. Commonly, NWP are formulated such that they include enhanced mixing to prevent excessive surface cooling (Sandu et al., 2013), also called 'runaway cooling'. This is implemented through the use of a stability function which ensures that turbulence is artificially sustained even under very stable conditions. This type of stability function is called a long-tail stability function. However, these types of stability functions smooth transitions, i.e. they prevent abrupt transitions (Baas et al., 2017; van de Wiel et al., 2017). On the other hand, Kähnert (2022) showed that when a short-tail stability function, which suppresses turbulence in very stable conditions, is used models can become locked in a vSBL until sufficiently strong forcing induces a transition.

In their paper van de Wiel et al. (2017) considered three types of stability functions, namely the cutoff, short-tail, and long-tail forms. In all cases, the bistability of the SBL was observed for some parameter values, but the structure of the bifurcation diagram varied significantly depending on the stability function. To include model uncertainty related to the stability function, wind forcing or unresolved processes the conceptual model by van de Wiel et al. (2017) is transformed from a deterministic model to a stochastic one. This stochastic model can then be reinterpreted as a gradient flow, in which the temperature inversion evolves according to an underlying energy potential. We highlight that the choice of the stability function has a large impact on the height of the potential barrier that the system has to cross to undergo a regime transition. Hence, the likelihood of noise-induced regime transitions in a model is highly sensitive to the choice of stability function. Although this is shown here in a highly simplified, conceptual model, this may have consequences in NWP, as the variability of unresolved degrees of freedom can induce abrupt regime transitions. This effect is lost with a long-tail stability function. Hence, we hypothesize that the combination of the variability of unresolved scales with a short-tail stability function may be necessary to enable sharp transitions. This is particularly relevant in Polar regions where the long-lived polar night can lead to a flow possibly evolving in the vicinity of the transition region for a long time. Therefore, enabling sharp transitions may be relevant for correctly estimating long-term statistics of surface fluxes. One way of including the variability of unresolved degrees of freedom is by exploring stochastic parameterizations (Berner et al., 2017). An example is the stochastic stability function which is defined



by Boyko and Vercauteren (2023b). The authors proposed a stochastic extension to MOST for a single-column model that can represent unsteady and intermittent turbulence. Similarly, to qualitatively reproduce temporally localized bursts of turbulence  
95 in the vSBL regime, we use a stochastic parameterization of the short-tail stability function in the form used by van de Wiel et al. (2017). This model randomization is used to study to what extent localized events can trigger regime transitions in the stable boundary layer.

In summary, we want to study the sensitivity of the SBL to perturbations that represent model uncertainty. Model uncertainty arises among other things due to unresolved processes in the model and forcing uncertainty. In addition, surface heterogeneity  
100 and non-stationary turbulent variables contradict the assumptions of MOST leading to uncertainty in the turbulence parameterization. We utilize a randomized version of the nonlinear model suggested by van de Wiel et al. (2017) to address the following research questions:

- To what extent does the choice of stability function affect the likelihood of a transition?
- How sensitive are regime transitions to different types of model uncertainty?
- 105 – How does the inclusion of turbulent bursts in the vSBL regime effect the timing of regime transition?

To tackle these questions, in section 2.1 the model by van de Wiel et al. (2017) is introduced in detail. Section 2.2 discusses the impact of the choice of stability function on the representation of regimes and regime transitions. Following that, section 2.3.1 presents a sensitivity analysis of regime transitions, analyzing the impact of model uncertainty due to small-scale fluctuations of unresolved processes. Additional randomization is then investigated in section 2.3.2, where the dynamical forcing  
110 variable, i.e. the geostrophic wind, is treated as a random variable. As the simplest scenario, we use an Ornstein-Uhlenbeck process to represent the random geostrophic wind forcing. Lastly, section 2.3.3 studies the impact of a randomized stability function. For this, the short-tail stability function by van de Wiel et al. (2017) is extended with multiplicative noise. We study how the timing of transitions changes related to the wind forcing with a randomized stability function.

## 2 Conceptual model for near-surface temperature inversions

### 115 2.1 Model description

In their study, van de Wiel et al. (2017) developed a conceptual model that describes the evolution of near-surface inversion strength over time. To achieve this, they combined a surface energy budget with a bulk model of the lower atmosphere and investigated near-surface temperature inversion transitions in the polar and nocturnal atmospheric boundary layer. The model highlights a nonlinear relationship between the stability of temperature inversion and ambient wind speed by employing a first-  
120 order ODE to represent the time evolution of the temperature differences,  $\Delta T$ , between a reference height ( $T_r$ ) and the surface temperature ( $T_s$ ). A brief summary of the model is given below, with more details available in van de Wiel et al. (2017).

Assuming a symmetry between the bulk temperature differences in the atmosphere and soil, the evolution of the temperature



inversion is governed by a surface energy balance:

$$\frac{d\Delta T}{dt} = \frac{1}{c_v}(Q_n - G - H) \quad (1)$$

125 where  $\Delta T = T_r - T_s$  is the inversion strength,  $c_v$  the heat capacity of the surface,  $Q_n$  the net longwave radiative flux,  $G$  the soil heat flux and  $H$  the turbulent sensible hat flux.

After parameterizing the fluxes, the model takes the form:

$$\frac{d\Delta T}{dt} = \frac{1}{c_v}(Q_i - \lambda\Delta T - \rho c_p c_D U \Delta T f_{\text{stab}}(R_b)), \quad R_b = z_r \frac{g\Delta T}{T_r U^2} \quad (2)$$

130 where  $R_b$  is the bulk Richardson number,  $Q_i$  represents the isothermal net radiation,  $\lambda$  the net linear effect of all feedbacks from soil heat conduction and radiative cooling represented with a lumped parameter,  $\rho$  stands for the density of air at constant pressure and  $c_p$  is the heat capacity of air at constant pressure. Additionally,  $c_D = (\frac{\kappa}{\ln(z_r/z_0)})^2$  is referred to as the neutral drag coefficient where  $\kappa$  is approximately equal to 0.4 and the von Kármán constant,  $z_0$  the roughness length and  $z_r$  the reference height. Moreover,  $U$  represents the wind speed at height  $z_r$ . The sensible heat flux  $H$  is parameterized with Monin-Obukhov similarity theory which is using a stability function,  $f_{\text{stab}}(R_b)$ , to describe how much turbulence is present in relation to the  
135 strength of the stratification.

Based on the observation that the wind speed was constant at a certain height (Hooijdonk et al., 2015), the model assumes that the wind speed and temperature are constant at reference height  $z_r$ . The same values as in van de Wiel et al. (2017) (Table 1, Dome C) are used for all parameters unless stated otherwise. For convenience, all parameter values are summarized in Table 1. The Dome C data was collected at the Concordia Research Station located on the Antarctica Plateau. This French-Italian  
140 research facility, situated at an elevation of 3,233m above sea level, is described in detail by Genthon et al. (2010). The data from 2017, consisting of 10-minute averaged meteorological data, is for example analyzed by Vignon et al. (2017) and Baas et al. (2019). In our study the focus lies on the polar night, which lasts from March to September, and the following parameters are crucial: the temperature at 9.4m height and the surface, the wind speed ( $\text{ms}^{-1}$ ) at 8m height, and the radiation in the polar night. Following van de Wiel et al. (2017), only the data where the radiative forcing ( $R^+ = SW^\downarrow - SW^\uparrow + LW^\downarrow$ ) is less than  
145  $80 \text{ Wm}^{-2}$  is considered when the data is studied.  $SW^\downarrow$  is the incoming and  $SW^\uparrow$  the outgoing shortwave radiation and  $LW^\downarrow$  the incoming longwave radiation. For  $R^+ < 80 \text{ Wm}^{-2}$  the sky is very clear (Vignon et al., 2017) and cooling is pronounced.

The authors of the model (2) provide an in-depth analysis of the model's equilibrium states and their stability against perturbations. For the purpose of this study, the most important features of the model are that the solution is bistable with the above-mentioned parameters. This means that, for specific wind speeds  $U$ , the model has two stable equilibrium solutions  
150 and an unstable one. Transitions between stable states can be triggered by large enough perturbations. Figure 1 c) shows the locations of the stable states for the discussed model driven by the parameters given in table 1. The blue line is a plot of the equilibrium solutions of the parameterized model by van de Wiel et al. (2017) (i.e. equation 2). For low wind speeds and high-temperature difference, there is one regime of stable equilibria and an additional one for high  $U$  and small  $\Delta T$ . They are marked with a solid line. In between those two stable regimes there is a  $U$  regime with unstable equilibria (dotted line).  
155 Connecting this to the SBL context the first stable regime is one with very stable stratification while the other one is weakly



parameter	value	unit
$Q_i$	50.0	$Wm^{-2}$
$\lambda$	2.0	$Wm^{-2}K^{-1}$
$\kappa$	0.4	-
$c_v$	1000	$Jm^{-2}K^{-1}$ ?
$\rho$	1.0	$kgm^{-3}$
$c_p$	1005.0	$Jkg^{-1}K^{-1}$
$z_0$	0.01	m
$z_r$	10.0	m
$U$	5.2	$ms^{-1}$
$g$	9.81	$ms^{-2}$
$T_r$	243.0	K
$\alpha$	5.0	-

**Table 1.** Default parameter values for the model (i.e. eq. 2).

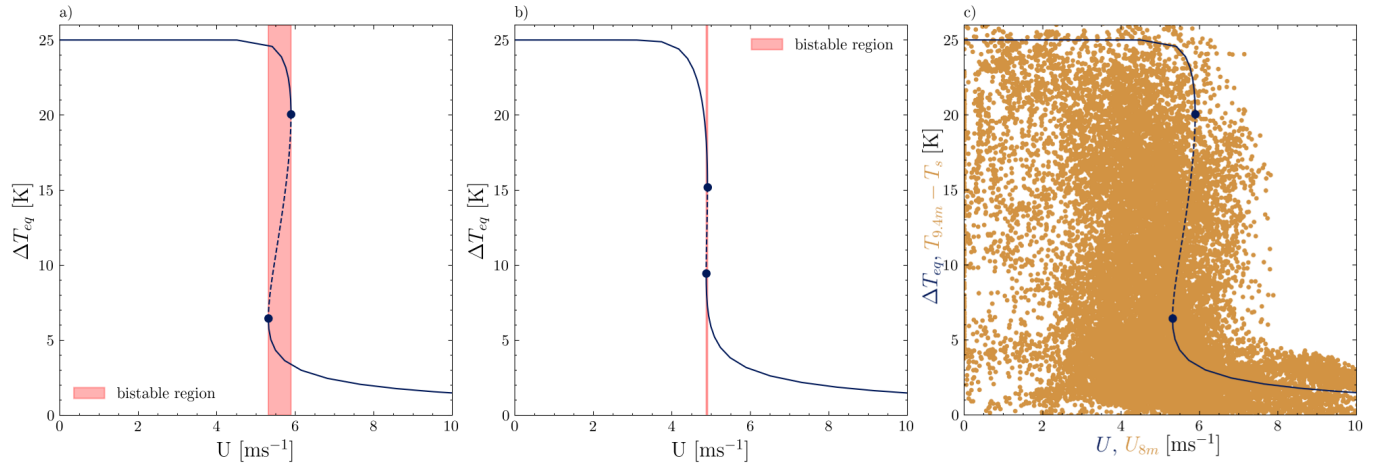


**Figure 1.** Equilibrium points of the model with a a) short-tail and b) long-tail stability function plotted over wind speed. The dotted lines mark unstable equilibria while the solid lines correspond to stable ones. The red region is the region with two possible solutions for the same forcing conditions. In plot c) the orange dots are observational data from Dome C and the blue line corresponds to the equilibrium solutions of the model with a short-tail stability function.

stable. As noted by van de Wiel et al. (2017), a similar behavior is apparent in observational data for example measured at Dome C. When plotting  $\Delta T = T_{9.4m} - T_s$  against the wind speed  $U_{8m}$  a back-folding of the points becomes discernible when  $R^+ < 80 Wm^{-2}$  (as shown in van de Wiel et al. (2017), Fig. 6 and less clearly in our figure 1 c)). In figure 1 c) the orange dots are the described 10-minute averaged observational data from Dome C. In the data, a weakly stable regime is clearly



160 observable but the very stable regime is not as distinct. As shown by van de Wiel et al. (2017) and in figure 1 c), the model provides a qualitative representation of the data at Dome C, particularly regarding the existence of two limiting states. Based on that, the model is chosen to study transitions in the polar SBL.

## 2.2 Impact of the choice of the stability function

In MOST the strength of turbulence, depending on the dimensionless stability of the flow, is given by the mixing length which is adjusted through a stability function (Foken, 2006). The choice of stability function has a large impact on the parameterization of turbulence. Under strong stratification, long-tail stability functions allow turbulence to exist while with a short-tail stability function, turbulence is largely suppressed after a critical Richardson number. Long-tail stability functions are typically utilized in NWP to avoid excessive cooling in highly stable conditions within the SBL (Sandu et al., 2013; van de Wiel et al., 2002). The use of such stability functions however has broader consequences and strongly influences the representation of transitions between SBL regimes. By artificially sustaining turbulence even under very stable conditions the transitions become less abrupt (Baas et al., 2017). Further impacts of the stability function on the representation of the bistability of the system are analyzed here, focusing on the likelihood of regime transitions when model uncertainty is present. Analogous to van de Wiel et al. (2017) we use  $f_{stab}(R_b) = \exp(-2\alpha R_b)$  as a long-tail stability function and  $f_{stab}(R_b) = \exp(-2\alpha R_b - (\alpha R_b)^2)$  as a short-tail one with  $\alpha = 5$ . Both short-tail and long-tail stability functions are plotted in Figure 2. For a Richardson number larger than 0.35 the short-tail stability function is approaching zero.

As we assume that not all degrees of freedom are represented in the conceptual model by van de Wiel et al. (2017), which leads to inherent model uncertainty the model, is transformed from a deterministic one to a stochastic one. The different types of randomization are given in detail in sections 2.3.1, 2.3.2 and 2.3.3. The likelihood of transitioning between the two stable states, in the context of noise-induced tipping, is very dependent on the choice of stability function. There are two main reasons for that. Firstly, the bistable range of wind speed is much narrower when using the long-tail stability function. This can be seen in figure 1. The bistable range is the region in which the model can have two stable solutions for the same forcing, i.e.  $U$ . For the short-tail stability function the bistable region spans from  $U = 5.31$  to  $5.89$  (figure 1 a) while for the long-tail stability function it is between  $4.87$  and  $4.9$  (figure 1 b). That means that the bistable region for the long-tail stability function has only 6% of the width of the one for the short-tail stability function. Therefore, with a long-tail stability function it is significantly less likely to transition from one stable regime to the other. This agrees with the findings of Baas et al. (2017). They show that enhanced mixing, which is the effect of a long-tail stability function, is detrimental for modeling the SBL. For example, near-surface cooling and wind shear are systematically underestimated with the enhanced mixing model. Secondly, to explain why the likelihood of transition is very dependent on the choice of stability function we introduce the concept of a potential. For this equation (2) can be rewritten as a stochastic gradient system

$$190 \quad \frac{d\Delta T}{dt} = -V'(\Delta T), \quad \Delta T(t_0) = \Delta T_0$$

where  $V : \mathbb{R} \rightarrow \mathbb{R}$  is an underlying potential influencing the dynamics of the temperature inversion. The extrema of the potential  $V$  correspond to the equilibria of  $\Delta T$ , i.e. for an equilibrium point  $\Delta T_e$  it holds  $V'(\Delta T_e) = 0$ . Using figure 3 we can compare



the potentials for a short-tail stability function (figure 3 a) and a long-tail one (figure 3 b). The lines correspond to potentials for different wind speeds which are in the bistable region. The green histograms are the results of 1000 simulations of the model where the model itself is randomized similarly to Kaiser et al. (2020) (for a detailed description of the randomization see section 2.3.1). All simulations were started in the very stable regime, i.e.  $\Delta T_0 = 24$  K. In the short-tail stability function histogram the two stable equilibria ( $\Delta T = 4$  and 24 K) distinctively show up and there are clearly multiple transitions between both regimes. In contrast, for the long-tail stability function the very stable regime is not distinctively separated from the unstable one (located at  $\Delta T = 12$ K). This is related to the fact that the potential barrier is much shallower with the long-tail stability function. The potential barrier is the difference between the minima and maxima of the potential. Hence, this barrier needs to be overcome to transition to the second stable equilibrium. Even though there are multiple transitions between the two stable regimes with the long-tail stability function, the system rarely stays in the very stable regime leading to an under-representation of very stable stratification cases in the model. Based on these results we hypothesize that by using a randomized short-tail stability function instead of the enhanced mixing of the long-tail stability function transitions are better represented. In section 2.3.3 the stochastic stability function is introduced. This randomized parameterization accommodates the representation of transient bursts of turbulent mixing, which could force the system to transition.

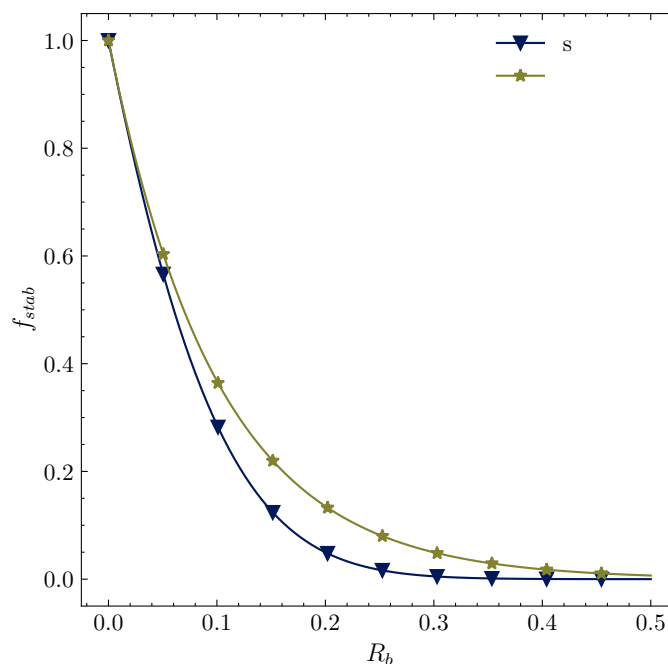


**Figure 2.** Long-tail and short-tail stability functions considered for the model plotted over the Richardson number.

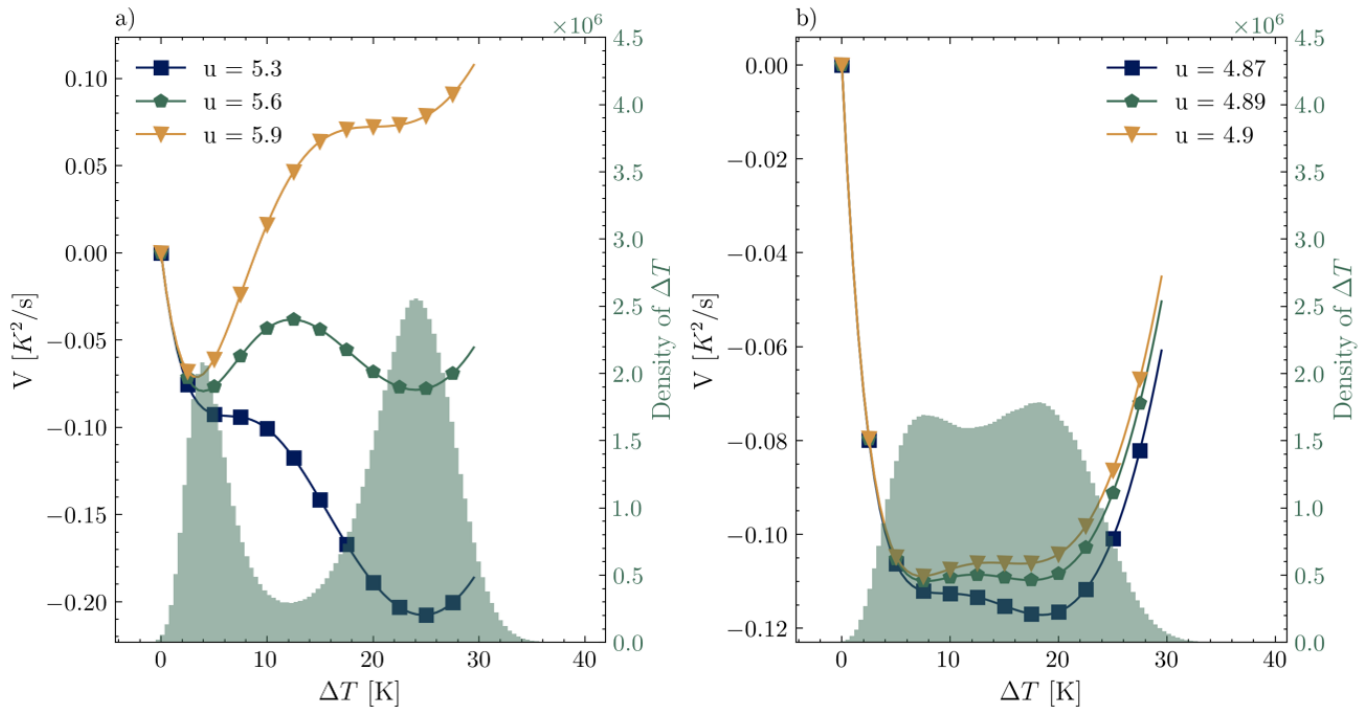


**Figure 3.** Potentials with a) short-tail and b) long-tail stability function for several wind speeds  $U$  and histograms of the results of 1000 simulations of the model with randomized wind speeds. In plot a) the mean of the random wind speed is equal to  $5.6 \text{ ms}^{-1}$  and in plot b) to  $4.89$ .

### 2.3 Randomization strategies

Three strategies are employed to address model uncertainty in the conceptual model proposed by van de Wiel et al. (2017) (eq. 2). Firstly, to account for uncertainty arising from unresolved processes within the model, a stochastic differential equation (SDE) version of the model is presented in section 2.3.1. Moreover, uncertainty related to the wind forcing is addressed in section 2.3.2 by modeling the wind with an Ornstein-Uhlenbeck process. This section also investigates the combined effect of randomizing the wind forcing and the model itself. Lastly, the study explores a randomized stability function as a potential solution to account for uncertainty in the parameterization of turbulence. A stochastic stability function allows the inclusion of turbulent bursts even in very stable stratification. In all cases, the aim is to account for small-scale fluctuations rather than large-scale changes. As van de Wiel et al. (2017) showed that their model, in its deterministic form, is highly sensitive to a change in the lumped parameter,  $\lambda$ , which represents soil and radiation feedbacks and the surface roughness,  $z_0$ , both parameters are not further investigated in this study.

Stochastic parameterizations have the merit to provide uncertainty estimations, but beyond that they have the potential to induce regime transitions if the physical system has multiple coexisting equilibria. In that sense, they may be necessary for better representing the mean state of the system (Berner et al., 2017). Here the stochastic modeling will be used to study the



effect of small-scale fluctuations of an unresolved process in the model, the wind speed or to include localized turbulent bursts. A sensitivity analysis will be carried out to comprehend and discern the impacts of the aforementioned model uncertainties. Through the utilization of this tool, we aim to enhance our comprehension of which of these model uncertainties have a large impact on the statistical representation of regimes and transitions between them.

225 Due to the presence of noise, the equilibrium points of the deterministic and random model will not exactly be the same but the dominant effects will be. The impact of noise in the model is quantified based on a Monte Carlo simulation with 500 realizations. A comparison with 1000 simulations showed similar results. Hence, 500 realizations are deemed sufficient for the rest of the sensitivity analysis. For all simulations the simulation time is 24 hours and time steps have a length of 1 second. Moreover, model parameters are the same as in table 1. All SDEs are solved using the function `itoint` from the python library `sdeint` by Aburn. This function applies the stochastic Runge-Kutta algorithm of order 1.0 (Rößler, 2010).

### 2.3.1 Internal variability

Many processes are not resolved in the simplified conceptual model by van de Wiel et al. (2017) (eq. 2). In a first randomization strategy, a stochastic term is added to the model to represent small-scale fluctuations of the dynamics of the temperature inversion due to unresolved processes. The goal is to quantify the impact of model uncertainties as an additive noise component on the statistical representation of regimes in the SBL. The model is defined as

$$d\Delta T = \frac{1}{c_v} (Q_i - \lambda\Delta T - \rho c_p c_D U \Delta T f_{\text{stab}}(R_b)) dt + \sigma_i dW_i, \quad \Delta T_0 = x_0 \quad (3)$$

where  $W_i$  is a Wiener process (i.e. stochastic process),  $\sigma_i$  scales the fluctuation intensity, and  $x_0$  is either equal to 4K (wSBL) or 24K (vSBL).

To assess the model's response to this randomization, a sensitivity analysis is conducted and the focus is placed on the representation of regime transitions (see figure 4). The adapted equation (3) of the model (2) is run 500 times for each combination of a range of different  $U$  and  $\sigma_i$  values. To distinguish the effect of the randomization on the two transition types the simulations are started in the vSBL state, i.e.  $\Delta T_0 = 24\text{K}$ , and in the wSBL one,  $\Delta T_0 = 4\text{K}$ . Then for every  $U$  the minimal  $\sigma_i$ , for which at least 80% of all 24-hour simulations include at least one transition, is identified. For convenience, this minimal  $\sigma_i$  is abbreviated as  $\sigma_{i,\text{min}}$ . As anticipated, the value of  $\sigma_{i,\text{min}}$  to achieve transitions from wSBL to vSBL is low for low wind speeds and higher for high winds. Conversely, for transitions from vSBL to wSBL, the opposite trend is observed. This phenomenon can be explained by examining the plot of the equilibrium points for the deterministic model (eq. 2) (see the dotted red line in figure 4). At low wind speeds the system has a single equilibrium state which is the vSBL. Consequently, only a small amplitude of noise is necessary to transition from wSBL to vSBL, while a higher amplitude is required to exit vSBL and transition to wSBL. In the bistable region two stable equilibrium states are present for the same  $U$  value. In the first segment of the bistable region the wSBL and vSBL  $\sigma_{i,\text{min}}$  converge until they are nearly identical for  $U = 5.6 \text{ ms}^{-1}$ . At this point, the unstable equilibrium state is positioned approximately midway between the two stable states. Consequently, the same noise magnitude is required for transitions in both directions. Subsequently, as the wind speed increases, the two  $\sigma_{i,\text{min}}$  diverge again. Here, the reverse argument can be made in comparison to low wind speeds: only a small amplitude of noise is necessary

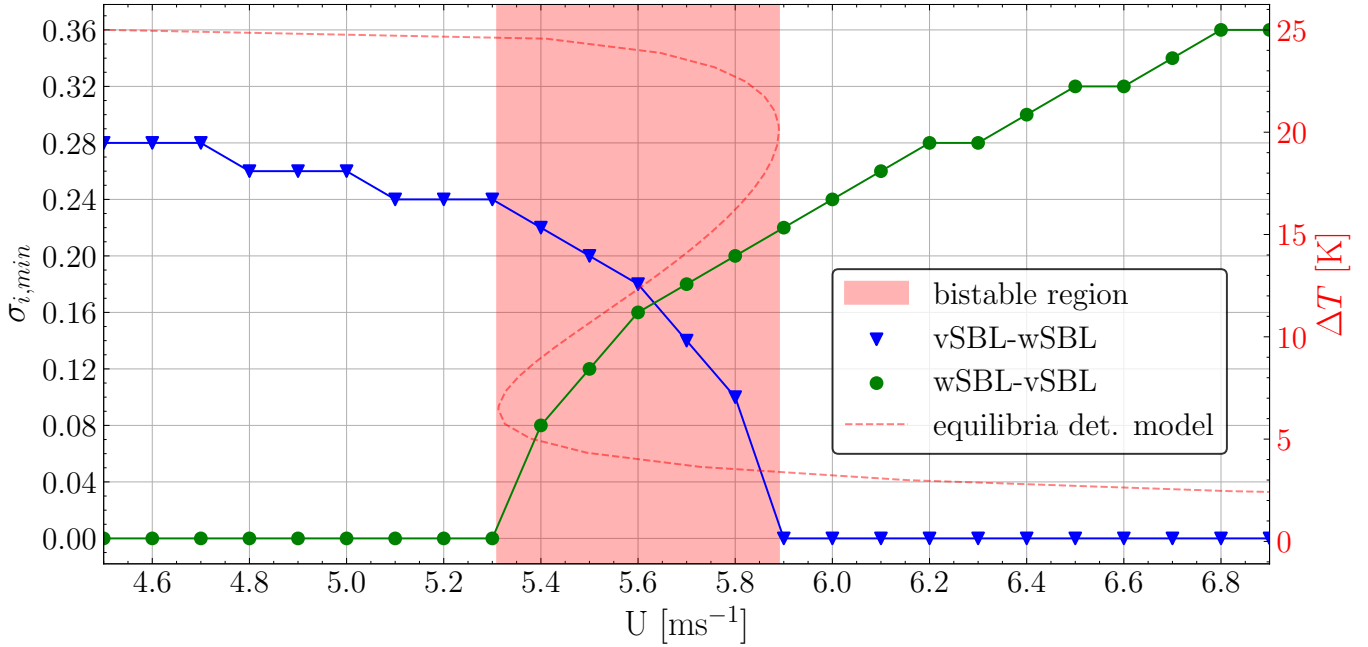


**Figure 4.** Results of the sensitivity study of model (3). For every  $U$  the minimal  $\sigma_i$  ( $\sigma_{i,min}$ ) for which at least 80% of the 500 simulations have at least one transition of the indicated type is marked. Simulations with an initial condition  $\Delta T_0 = 24\text{K}$  are plotted in green and with  $\Delta T_0 = 4\text{K}$  in blue. The red line is the bifurcation diagram of the deterministic model (eq. 2) and its bifurcation region is the red shaded area.

to transition to the wSBL state since it represents the sole equilibrium state of the system and higher noise values are required to exit this state and transition to the vSBL state. As the bifurcation diagram is not exactly symmetric higher noise levels for wSBL to vSBL transitions and high  $U$  values are required than for vSBL to wSBL transitions and low  $U$  values. This rationale is justified as small-scale turbulent bursts may introduce enough mixing to force a transition to the wSBL state, whereas the inverse scenario does not hold true. Based on this discussion, it can be deduced that only a small noise amplitude is required for the system to transition to its equilibrium state (vSBL for low wind speeds and wSBL for high wind speeds). However, to depart from the equilibrium state, higher noise amplitudes are necessary. Within the bistable region, the introduction of noise with small amplitudes allows transitions in both directions.

To illustrate the effect of the randomization in the model an example is shown for the symmetry wind speed  $U = 5.6 \text{ ms}^{-1}$ . In this case,  $\sigma_{i,min}$  is equal to 0.18 for transitions from vSBL to wSBL which is slightly larger than for transitions in the other direction. The simulation is started in the vSBL regime. Figure 5 displays an instance of one model run with  $\sigma_i = 0.18$  and  $U = 5.6 \text{ ms}^{-1}$ . The stable equilibria of the deterministic model are indicated by two solid red lines, while the location of the unstable equilibrium is marked by a dotted line. This specific model run exhibits two transitions between the vSBL and wSBL regimes. It is important to note that, in the absence of noise, the system would remain in the very stable regime and not undergo any transitions.

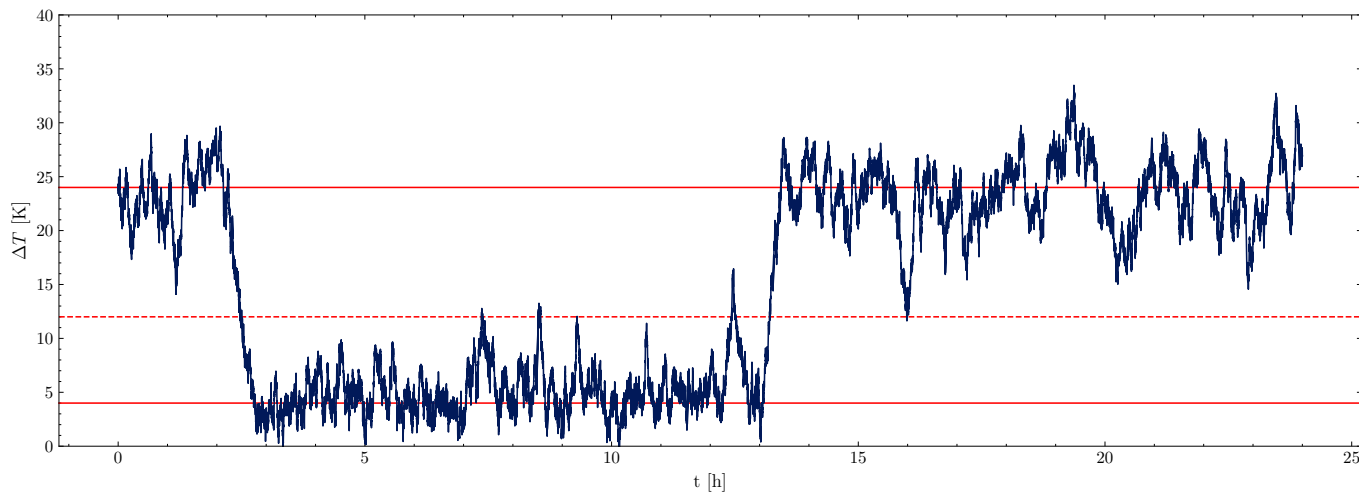


**Figure 5.** Plot of one solution of equation 3 with  $U = 5.6 \text{ ms}^{-1}$  and  $\sigma_i = 0.18$ . The red dotted line marks the unstable equilibria of the deterministic model while the solid lines correspond to stable ones.

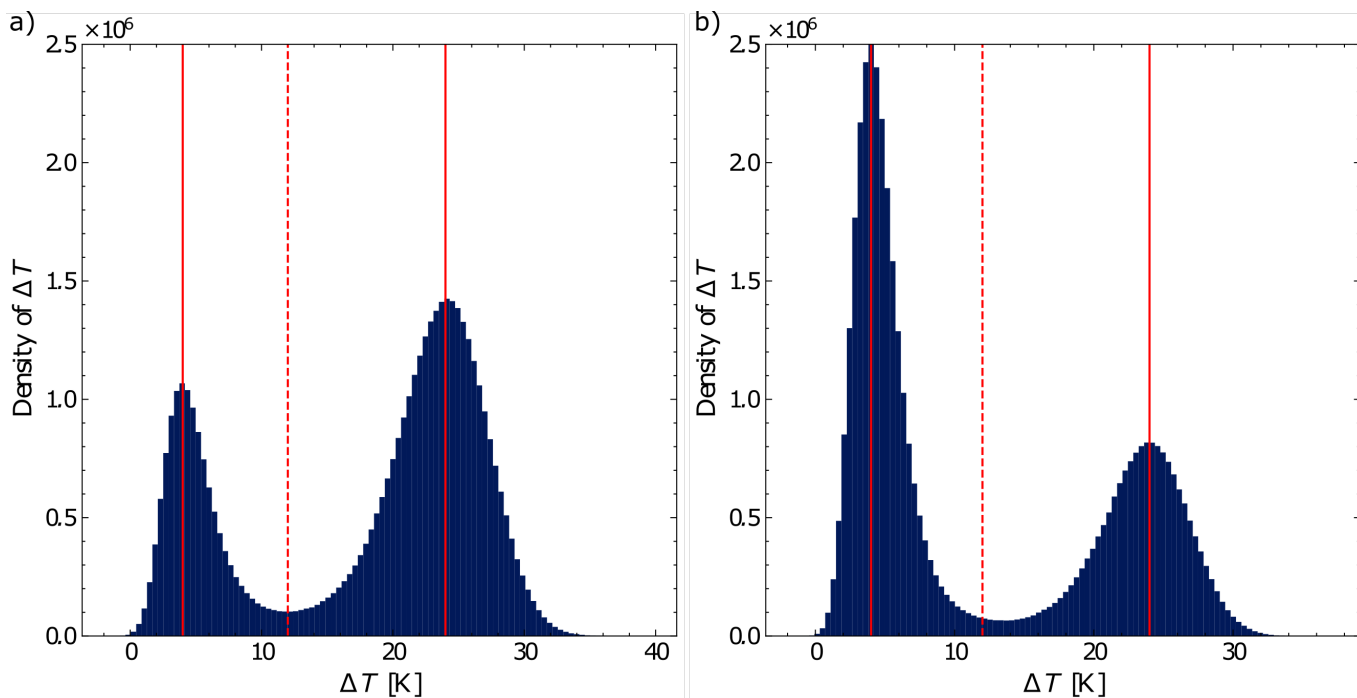


**Figure 6.** Histogram of all solutions of equation 3 with  $U = 5.6 \text{ ms}^{-1}$  and a)  $\sigma_i = 0.18$ ,  $\Delta T_0 = 24\text{K}$  and b)  $\sigma_i = 0.16$ ,  $\Delta T_0 = 4\text{K}$ . The red horizontal dotted line marks the unstable equilibria of the deterministic model while the solid lines correspond to stable ones.



270 Lastly, to give an example of how the randomization affects the model result statistically the histogram of  $\Delta T$  for 500 model runs for  $U = 5.6 \text{ ms}^{-1}$  is shown in figure 6. For plot a) all the simulations are started in the vSBL and for plot b) in the wSBL. The  $\sigma_i$  are the corresponding  $\sigma_{i,min}$  from figure 4. For both simulation types the histogram shows a higher probability to be in the regime where the simulation started. This effect is especially pronounced for the simulations which started in the wSBL state.

### 2.3.2 Fluctuating wind speed

275 A narrow wind speed range exists in which a sudden change in the temperature inversion can be observed (e.g. Baas et al. (2019), see also Fig. 1 c)). To investigate when small variations of forcing wind speed can lead to sharp transitions, the conceptual model is modified by randomizing  $U$  such that it fluctuates around a wind speed for which the system is bistable. To simulate the fluctuating wind speed, an Ornstein-Uhlenbeck process is incorporated into the model. This process is a widely used stochastic process in various applications (Pavliotis, 2014). The randomized model is defined as follows:

$$280 \quad \begin{aligned} d\Delta T &= \frac{1}{c_v} (Q_i - \lambda \Delta T - \rho c_p c_D U \Delta T f_{\text{stab}}(R_b)) dt, \quad \Delta T_0 = x_0, \\ dU &= -r(U - \bar{U}) dt + \sigma_U dW_U, \quad U_0 = 5.6, \end{aligned} \quad (4)$$

where  $r$  is a relaxation or mean reversion term. The value of  $r$  is chosen to be 0.005 for all simulations to achieve a mean reversion time of 200 s which is roughly the order of a submesoscale motion (Vercauteren et al., 2016). The value of  $x_0$  is either equal to 4K (wSBL) or 24K (vSBL). The asymptotic mean of the Ornstein-Uhlenbeck process,  $\bar{U}$ , is set to  $5.6 \text{ ms}^{-1}$  as this is the middle of the bistable region (see section 2.2). Different parameter values may give a different quantitative result but we expect them to be qualitative the same. The asymptotic variance of the Ornstein-Uhlenbeck process is  $\mathbb{V}(U) = \frac{\sigma_U^2}{2r}$  (Pavliotis, 2014). The value for  $\sigma_U$  is chosen based on 30-minute averaged observational data from Dome C (Genthon et al., 2021). In their study Baas et al. (2019) defined the bistable region for Dome C as  $4 \text{ ms}^{-1} \leq U \leq 7 \text{ ms}^{-1}$ . By using the same thresholds and using data from the year 2013, which has a mean value for the wind speed of  $5.6 \text{ ms}^{-1}$ , it can be deduced that  $\sigma_U$  should be equal to 0.08. Choosing  $\sigma_U$  this big leads to high variations in  $U$  and not to the small-scale perturbations we are interested in. Therefore, the value extrapolated from the Dome C data is only used as an indication of the order of magnitude of  $\sigma_U$  and additional values are tested. Figure 7 a) shows that while for  $\sigma_U = 0.01$  the fluctuations of  $U$  are of small amplitude and seldomly pass through a bifurcation point the time series does not transition. In fact, no simulation of all 500 includes a transition. In contrast, for  $\sigma_U = 0.04$  at least 80% of the simulations include a transition. This is the smallest  $\sigma_U$  which fulfills this condition. But in this case  $U$  no longer stays in the bistable region (see figure 7 b)).

295 As a next step, a model with both additive noise for internal variability and an Ornstein-Uhlenbeck process for wind velocity is considered. This model is defined as:

$$\begin{aligned} d\Delta T &= \frac{1}{c_v} (Q_i - \lambda \Delta T - \rho c_p c_D U \Delta T f_{\text{stab}}(R_b)) dt + \sigma_i dW_i, \quad \Delta T_0 = x, \\ dU &= -r(U - \bar{U}) dt + \sigma_U dW_U, \quad U_0 = 5.6. \end{aligned} \quad (5)$$

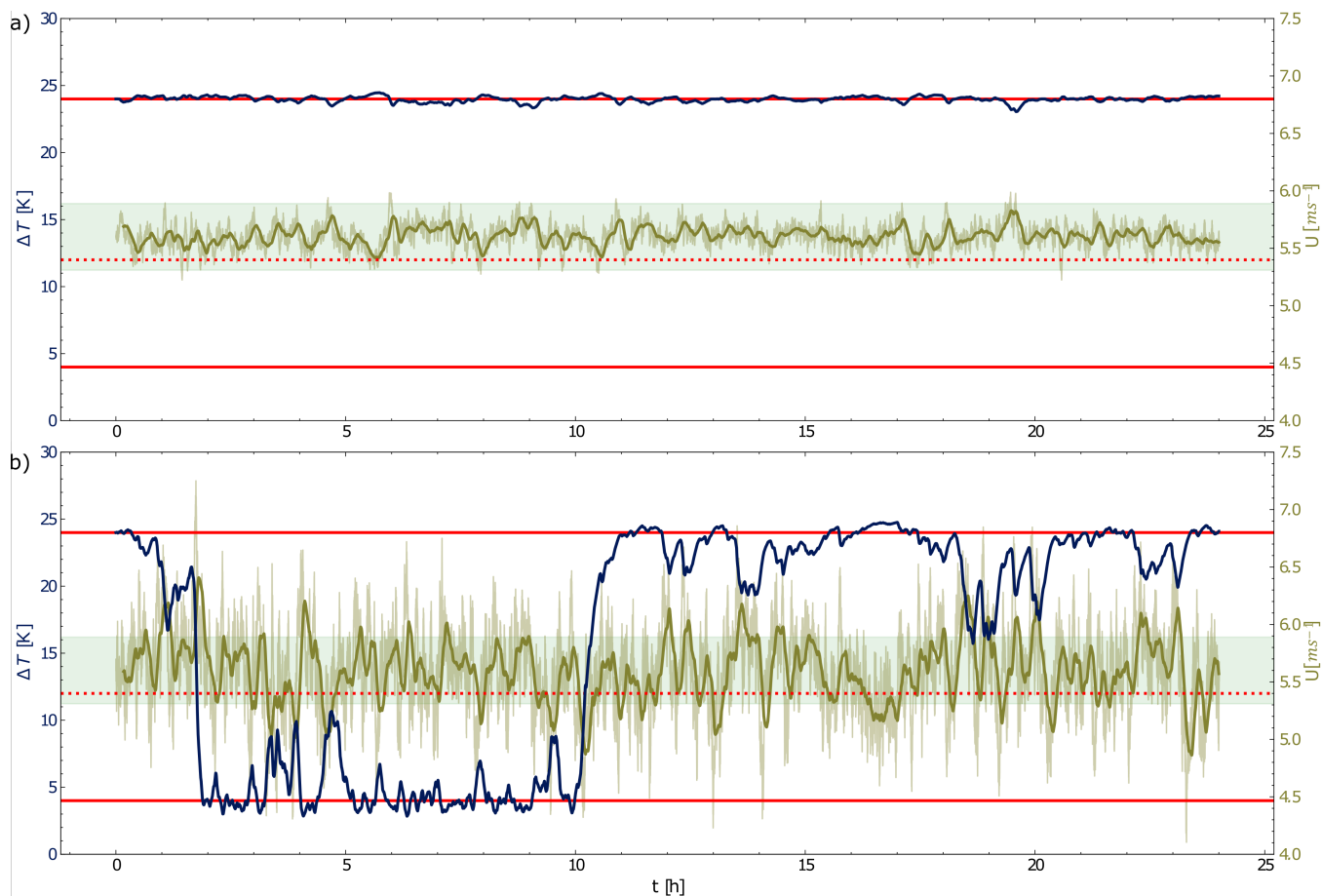


**Figure 7.** Plot of one solution of equation 4 (blue) and the corresponding wind speed  $U$  (green) including its 10-minute average (thick green line) for  $\sigma_U = 0.01$  (a) and  $\sigma_U = 0.04$  (b). The red dotted line marks the unstable equilibria of the deterministic model while the solid lines correspond to the stable ones. The shaded green area is the bistable region for  $U$ .

The relaxation parameter  $r$  is the same as before. To quantify the impact of this model randomization, in terms of regime transitions, a sensitivity analysis is performed (see figure 8). The model (5) is run 500 times for a combination of  $\sigma_i$ ,  $\sigma_U$  and  $U$  values. For  $\sigma_U$  the values 0, 0.01 and 0.04 are chosen to allow a comparison of the results with the ones with the model where only the wind velocity is randomized (see eq. 4). It shall be noted that when  $\sigma_U = 0$  model (5) is behaviourally equal to model (3). The simulations are started in the vSBL state,  $\Delta T_0 = 24\text{K}$ , (blue lines) and in the wSBL one,  $\Delta T_0 = 4\text{K}$ , (green lines) to distinguish the effects on the two transition types separately. Then the minimal  $\sigma_i$  for which at least 80% of all simulations with the given  $\sigma_U$  and  $U$  value include at least one transition is identified. This  $\sigma_i$  is abbreviated as  $\sigma_{i,min}$ .

305 Comparable with the results of model (3), where solely unresolved processes were considered while disregarding fluctuating wind speed, figure 8 shows that no noise is required for the system to transition to its equilibrium state (vSBL for low wind speeds and wSBL for high wind speeds). However, to depart from the equilibrium state, higher noise amplitudes are necessary.

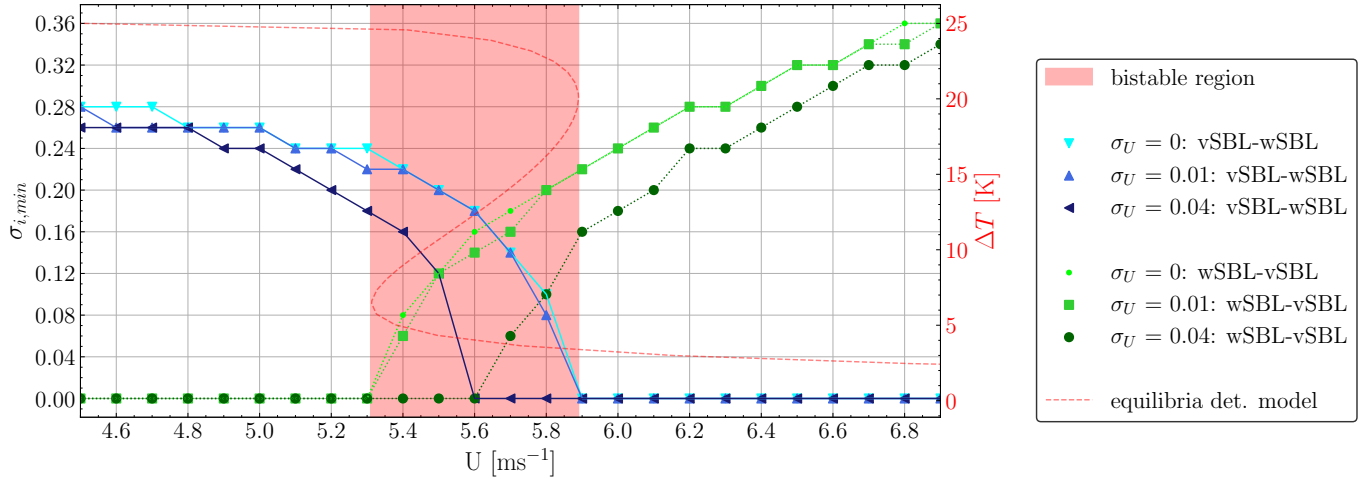


**Figure 8.** Results of the sensitivity study of model (5). For every  $U$  the minimal  $\sigma_i$  ( $\sigma_{i,min}$ ) for which at least 80% of the 500 simulations have at least one transition of the indicated type is marked. Simulations with an initial condition  $\Delta T_0 = 24\text{K}$  are plotted in green and with  $\Delta T_0 = 4\text{K}$  in blue. The red line is the bifurcation diagram of the deterministic model (eq. 2) and its bifurcation region is the red shaded area.

In the bistable region, the introduction of noise with small amplitudes enables transitions in both directions, irrespective of the three different  $\sigma_U$  values. Notably, larger  $\sigma_U$  values permit smaller  $\sigma_i$  values to induce transitions. This is especially pronounced when  $U = 5.6\text{ms}^{-1}$  and  $\sigma_U = 0.04$ . In this case  $\sigma_{i,min}$  is equal to zero for both transition directions. The values of  $\sigma_{i,min}$  are identical or nearly identical for  $\sigma_U = 0$  and 0.01.

Additionally, to provide a statistical representation of the model’s randomization effects on the results, histograms of  $\Delta T$  for 500 model runs with  $U = 5.6\text{ms}^{-1}$  and  $\sigma_U = 0.01$  is presented in figure 9. For plot a) all the simulations are started in the vSBL and for plot b) in the wSBL. The  $\sigma_i$  are the corresponding  $\sigma_{i,min}$  from figure 8. The histograms reveal a higher probability of remaining within the initial regime for both simulation types, with a more pronounced effect observed for simulations starting in the wSBL state.

### 2.3.3 Randomized stability function

In the conceptual model by van de Wiel et al. (2017) (eq. 1) the sensible heat flux is parameterized using MOST which uses the assumption that turbulence is stationary. In the vSBL regime, this assumption does not hold and turbulence is rather intermittent and unsteady (Liang et al., 2014; Mahrt and Bou-Zeid, 2020). Therefore, in this section the impact of uncertainties in the turbulence parameterization is studied. This is particularly significant as localized turbulent events can trigger regime transitions in the stable boundary layer (Lan et al., 2022). To qualitatively reproduce continuous bursts of turbulence a model is introduced which enables temporally localized enhancement of turbulence. This is achieved by enhancing the mixing length. In MOST the mixing length is adjusted through a stability correction function. Therefore, a model is suggested where localized

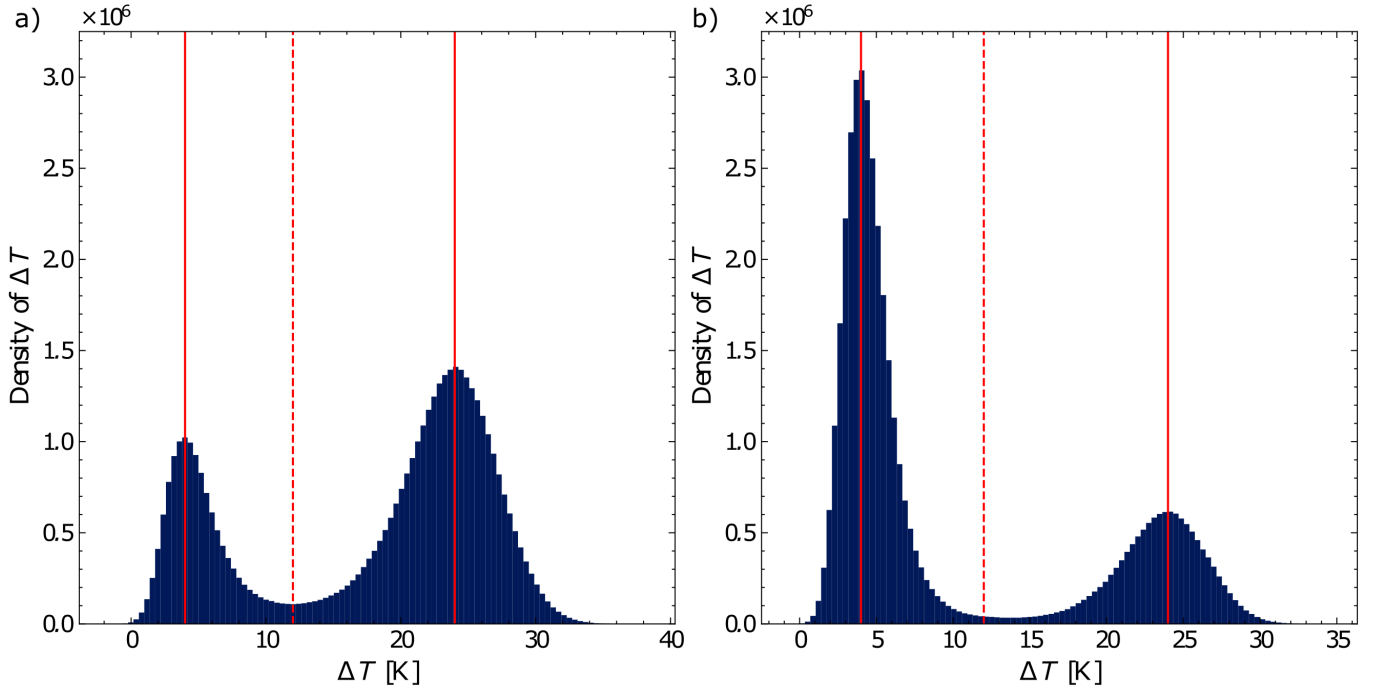


**Figure 9.** Histogram of all solutions of equation 5 with  $U = 5.6 \text{ ms}^{-1}$ ,  $\sigma_U = 0.01$  and a)  $\sigma_i = 0.18$ ,  $\Delta T_0 = 24\text{K}$  and b)  $\sigma_i = 0.14$ ,  $\Delta T_0 = 4\text{K}$ . The red horizontal dotted line marks the unstable equilibria of the deterministic model while the solid lines correspond to stable ones.

325 turbulence bursts are represented with a stochastic stability function. As the stability functions are the data-driven component of the MOST parameterization they are a natural choice for making part of the model random.

To account for localized bursts of turbulence the before mentioned short-tail stability function is extended with multiplicative noise. Using multiplicative noise ensures that the turbulent bursts are temporally localized, allowing the solution to relax towards that of the deterministic model after each burst. Additionally, unlike additive noise, the magnitude of the multiplicative noise depends on the current system state. Moreover, employing multiplicative noise instead of additive noise prevents the stability function from yielding negative values. Lastly, the model for the randomized stability function is chosen such that it includes a time memory to ensure that bursts of turbulence are not dispelled after one time step. The coupled system has the form

$$\begin{aligned}
 d\Delta T &= \frac{1}{c_v} (Q_i - \lambda\Delta T - \rho c_p c_D U \Delta T \phi) dt, \quad \Delta T_0 = x_0, \\
 d\phi &= -r(\phi - f_{stab}(R_b)) dt + \sigma_\phi \phi dW_\phi, \quad \phi_0 = f_{stab}(R_b(\Delta T_0)),
 \end{aligned}
 \tag{6}$$

335 with

$$\sigma_\phi = \begin{cases} 0 & R_b \leq Ri_c \\ c_\phi & \text{otherwise,} \end{cases}$$



340  $R_b$  is the bulk Richardson number,  $R_{i_c} = 0.25$  the critical Richardson number and  $c_\phi$  some constant which impacts the noise intensity. The noise is only non-zero for higher Richardson numbers as especially intermittent turbulence in the vSBL regime shall be accounted for in the model. The initial condition  $\phi_0$  is the value of the short-tail stability function corresponding to  $\Delta T_0$ . Again, to evaluate how the model reacts to this type of randomization, in relation to regime transitions, a sensitivity analysis is performed. The setup for the sensitivity analysis is the same as in section (2.3.1). That means, the model (6) is run 500 times for a combination of  $U$  and  $c_\phi$  values and the initial condition  $\Delta T_0$  is equal to 4 or 24K. Then, for each  $U$ , the minimum value of  $c_\phi$  is identified, which ensures that at least 80% of all 24-hour simulations include at least one transition. This minimum value is abbreviated as  $c_{\phi,min}$ .

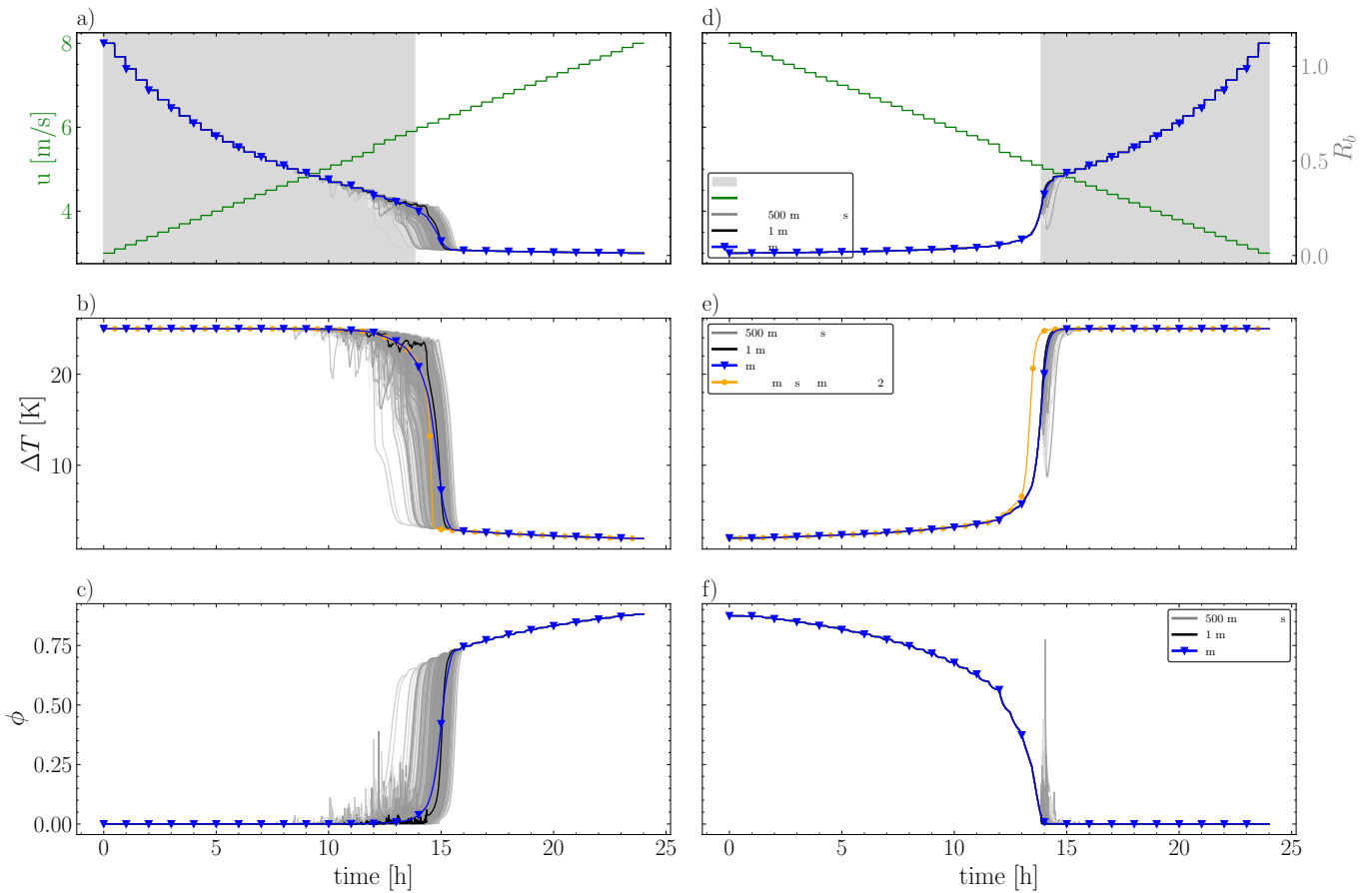


**Figure 10.** Solution of the model with perturbed stability function with variable forcing parameter  $U$  (wind velocity). Panel a) shows the time evolution of the forcing, panel b) of  $\Delta T$ , and c) of the stability function.

345 A similar sensitivity study as in section 2.3.1 and 2.3.2 was performed with 1000 model runs instead of 500 and for transitions from vSBL to wSBL. The results of this study are not shown here as for wind speeds less than  $5.3 \text{ ms}^{-1}$  even for high noise levels, e.g.  $c_\phi = 3$ , hardly any of the simulations included a transition. Our hypothesis is that this is due to that the model has



not enough degrees of freedom to non-linearly enhance the effect of the noise. We expect this to be different in a single-column model.

350 Lastly, the bifurcation driven transitions of the deterministic model are compared with the noise-induced transitions of the randomized model in figure 10. To achieve this the randomized model (6) is run 500 times with an incorporated time-varying wind forcing. The wind speed increases (left column) or decreases (right column) by  $0.1 \text{ ms}^{-1}$  roughly every 30 minutes as shown by the green curve in panel a). The effect of the randomization is studied for both transition types. Hence, the simulations either start in the vSBL state (left column) or the wSBL one (right column). Panel a) shows the time evolution of the forcing parameter  $U$  in green. The black line is the evolution of the bulk Richardson number for one simulation. The gray shaded area is the region where  $R_b > Ri_c$ . This is the region where noise is added to the stability function. Panel b) displays the time evolution of  $\Delta T$  with the forcing given in panel a). The gray lines correspond to 500 realizations of  $\Delta T$ . The black line is one realization of  $\Delta T$  with  $R_b$  as in panel a). The mean of all 500 simulations is given by the blue line. The orange line is the solution of the deterministic model (see equation 2) with  $U$  as given in panel a). Panel c) has the same color coding as panel b) 355  
360 only for  $\phi$  instead of  $\Delta T$ .

On average the deterministic model and the random simulations have the same transition time for transitions from vSBL to wSBL. However, with a randomized stability function, the transition time is no longer dependent on a specific wind velocity but allows for transitions to occur over a range of velocities before and after the transition of the deterministic model occurs. Therefore, the transition time becomes a range of roughly four hours instead of a fixed time point. The transitions start within 365 the wind speed range of  $5.5$  to  $6.25 \text{ ms}^{-1}$ . This observation aligns with the findings presented by (Baas et al., 2019), who demonstrated, through their analysis of observational data from Dome C, that wind speeds below approximately  $4 \text{ ms}^{-1}$  are associated with highly pronounced inversions ranging from 20 to 25 K. Conversely, wind speeds exceeding approximately  $7 \text{ ms}^{-1}$  correspond to comparatively weaker inversions on the order of 5 K. In contrast to vSBL to wSBL transitions, transitions from wSBL to vSBL are delayed compared to the deterministic model and occur over a narrow period.

370 Combining the results, it follows that the probability of transitions significantly increases with the use of a randomized short-tail stability function. Therefore, we suggest a modeling compromise where instead of the conventionally used long-tail stability function a stochastic parameterization, which includes random bursty features, is used. This alternative methodology has the potential to enhance the accuracy of large-scale statistics.

### 3 Summary and Conclusions

375 This study expands upon prior research by providing an explanation for the constraints encountered when depicting regime transitions in NWP. This is achieved by examining the significance of transient phenomena as triggers for abrupt transitions. We used a randomized version of the conceptual model defined by van de Wiel et al. (2017) as an exemplary model to study the sensitivity of the nocturnal or polar SBL to small-scale perturbations, and to investigate how related model uncertainty can impact the mean state of the boundary layer. The conceptual model by van de Wiel et al. (2017) is capable of accommodating



380 scenarios with multiple stable equilibria. Therefore, in relation to our objectives, it provides an ideal model for which the theoretical dynamical stability is well understood.

In the first part, we studied the impact of the stability function used in the model on the likelihood of regime transitions in the context of noise-induced tipping. We showed that for a short-tail stability function, in comparison to a long-tail one, the bistable region is significantly wider. In addition, the potential barrier for the long-tail stability function is shallower which decreases the chance for abrupt transitions. Combining both results we concluded that the stability function highly impacts the likelihood of transitions and that with a short-tail one the bistability of the system and abrupt transitions are better represented in the model. If NWP exhibit the regime bistability the usage of a long-tail stability function would lead to a smaller range of wind speeds for which transitions can occur due to the narrower bistable region. Moreover, the transitions would be smoothed out as a consequence of the shallower potential barrier. In contrast, a randomized short-tail stability function allows for noise-induced abrupt tipping.

In the second part, we analyzed how model uncertainty can be addressed in the conceptual model. We focused on model uncertainty related to unresolved processes, wind forcing, and turbulence parameterization. Firstly, to include small-scale perturbations of an unresolved process in the model it is extended with additive noise. To assess the model's response to this randomization, in terms of regime transitions, a sensitivity analysis was conducted. A Monte Carlo simulation with 500 runs and a combination of different wind speeds and noise strength was performed. Transitions from wSBL to vSBL and vice versa were studied separately. The sensitivity analysis showed that only a small noise amplitude is required for the system to transition to its equilibrium state (vSBL for low wind speeds and wSBL for high wind speeds). However, to depart from the equilibrium state, higher noise amplitudes are necessary. Within the bistable region, the introduction of noise with small amplitudes allows transitions in both directions. From this, we deduced that the model is highly sensitive to small-scale fluctuations of unresolved processes. Secondly, we studied the effect of including forcing uncertainty in the model by modeling the wind with an Ornstein-Uhlenbeck process. We showed that including randomized wind velocities which seldom exceed the bistable range was not sufficient to induce regime transitions. Therefore, we analyzed the impacts of including randomizations for unresolved processes and wind forcing together. Again a sensitivity analysis was performed. For low noise amplitudes of the randomized wind velocity, the results were nearly identical to the ones of the model where solely unresolved processes were considered. Lastly, to particularly address model uncertainty related to MOST we investigated how a commonly used stability function can be modified to represent unsteady turbulence often present in the SBL. MOST is based on the assumptions of surface homogeneity and turbulence stationarity which both have been shown to not always be valid. To relax this assumption and allow the representation of unsteady turbulence, we modified the short-tail stability function by van de Wiel et al. (2017) with a time memory and multiplicative noise. This is one way to represent localized turbulence bursts through a stochastic model. Moving forward, a natural progression would be designing a more sophisticated framework where the noise level is linked to the stratification level, since unsteady turbulence is known to mainly occur in high stratification. Such an approach has for example been pursued by Boyko and Vercauteren (2023a). The authors proposed a stochastic extension to MOST for a single-column model which scales with the Richardson number. The parameters of the stability correction were estimated based on observational data. A similar approach could be done for NWP or Earth system models to include localized turbulent



415 bursts. The inclusion of localized turbulence bursts is particularly significant as localized events can trigger regime transitions  
in the stable boundary layer. A randomized stability function offers an alternative way to mitigate excessive mixing resulting  
from a long-tail stability function (Baas et al., 2017), while preventing the system from being trapped in a highly stable state  
when using a short-tail stability function (Kähnert, 2022). We showed that by using a randomized stability function transitions  
from wSBL to vSBL are delayed. In contrast, transitions from vSBL to wSBL occurred both before and after the one from  
420 the purely deterministic model increasing thereby the transition period to four hours. Sun et al. (2012) separate the vSBL  
and wSBL regimes with a sharp wind speed threshold. With our finding this sharp threshold is extended to a range of wind  
speeds for which transitions are possible. Future research will entail studying the inclusion of the same and additional model  
uncertainties in a higher order model like a single-column model.

*Code and data availability.* The 30-minute averaged Dome C data which is used in this study can be accessed on PANGEA (see Genthon  
425 et al. (2021)). The source code to reproduce all results can be found here: [https://github.com/BoundaryLayerVercauteren/energy\\_balance\\_model](https://github.com/BoundaryLayerVercauteren/energy_balance_model)

*Author contributions.* All authors conceptualized the research project. The funding was acquired by NV. The methodology was developed  
by all authors. AK primarily performed the analysis and validation with support from NV and SK. AK developed the software. AK prepared  
the manuscript. All authors reviewed and edited the manuscript.

*Competing interests.* The authors declare that they have no conflict of interest.

430 *Acknowledgements.* This project has received funding from the European Union's Horizon 2020 research and innovation program under the  
Marie Skłodowska-Curie grant agreement number 945371. The authors thank Christophe Genthon and Etienne Vignon for providing the 10  
minute averaged Dome C data, obtained as part of the CALVA observation project supported by the French polar institute IPEV. Moreover,  
we wish to thank Peter Ashwin and Terje Koren Berntsen for helpful discussions.



## References

- 435 Abraham, C. and Monahan, A. H.: Climatological Features of the Weakly and Very Stably Stratified Nocturnal Boundary Layers. Part II: Regime Occupation and Transition Statistics and the Influence of External Drivers, *Journal of the Atmospheric Sciences*, 76, 3485–3504, <https://doi.org/10.1175/JAS-D-19-0078.1>, publisher: American Meteorological Society Section: Journal of the Atmospheric Sciences, 2019.
- Abraham, C., Holdsworth, A. M., and Monahan, A. H.: A prototype stochastic parameterization of regime behaviour in the stably stratified atmospheric boundary layer, *Nonlinear Processes in Geophysics*, 26, 401–427, <https://doi.org/10.5194/npg-26-401-2019>, publisher: Copernicus GmbH, 2019.
- 440 Aburn, M. J.: sdeint: Numerical integration of stochastic differential equations (SDE), <http://github.com/mattja/sdeint/>.
- Acevedo, O. C., Maroneze, R., Costa, F. D., Puhales, F. S., Degrazia, G. A., Nogueira Martins, L. G., Soares de Oliveira, P. E., and Mortarini, L.: The nocturnal boundary layer transition from weakly to very stable. Part I: Observations, *Quarterly Journal of the Royal Meteorological Society*, 145, 3577–3592, <https://doi.org/10.1002/qj.3642>, 2019.
- 445 Anson, C. and Mellado, J. P.: Global Intermittency and Collapsing Turbulence in the Stratified Planetary Boundary Layer, *Boundary-Layer Meteorology*, 153, 89–116, <https://doi.org/10.1007/s10546-014-9941-3>, publisher: Springer Netherlands, 2014.
- Ashwin, P., Wieczorek, S., Vitolo, R., and Cox, P.: Tipping points in open systems: bifurcation, noise-induced and rate-dependent examples in the climate system, *Philosophical Transactions of the Royal Society A: Mathematical, Physical and Engineering Sciences*, 370, 1166–1184, <https://doi.org/10.1098/rsta.2011.0306>, 2012.
- 450 Baas, P., van de Wiel, B. J. H., van der Linden, S. J. A., and Bosveld, F. C.: From near-neutral to strongly stratified: adequately modelling the clear-sky nocturnal boundary layer at Cabauw, *Boundary-Layer Meteorology*, 166, 217–238, <https://doi.org/10.1007/s10546-017-0304-8>, publisher: Springer Netherlands, 2017.
- Baas, P., van de Wiel, B. J. H., van Meijgaard, E., Vignon, E., Genthon, C., van der Linden, S. J. A., and de Roode, S. R.: Transitions in the wintertime near-surface temperature inversion at Dome C, Antarctica, *Quarterly Journal of the Royal Meteorological Society*, 145, 930–946, <https://doi.org/10.1002/qj.3450>, 2019.
- 455 Berner, J., Achatz, U., Batté, L., Bengtsson, L., Cámara, A. d. I., Christensen, H. M., Colangeli, M., Coleman, D. R. B., Crommelin, D., Dolaptchiev, S. I., Franzke, C. L. E., Friederichs, P., Imkeller, P., Järvinen, H., Juricke, S., Kitsios, V., Lott, F., Lucarini, V., Mahajan, S., Palmer, T. N., Penland, C., Sakradzija, M., Storch, J.-S. v., Weisheimer, A., Weniger, M., Williams, P. D., and Yano, J.-I.: Stochastic Parameterization: Toward a New View of Weather and Climate Models, *Bulletin of the American Meteorological Society*, 98, 565–588, <https://doi.org/10.1175/BAMS-D-15-00268.1>, publisher: American Meteorological Society Section: Bulletin of the American Meteorological Society, 2017.
- 460 Boyko, V. and Vercauteren, N.: Simulating the unsteady stable boundary layer with a stochastic stability equation, preprint, ESS Open Archive, <https://doi.org/10.22541/essoar.168614510.05701780/v1>, 2023a.
- 465 Boyko, V. and Vercauteren, N.: A stochastic stability equation for unsteady turbulence in the stable boundary layer, *Quarterly Journal of the Royal Meteorological Society*, n/a, <https://doi.org/10.1002/qj.4498>, 2023b.
- Cuxart, J., Holtlag, A., Beare, R. J., Bazile, E., Beljaars, A., Cheng, A., Conangla, L., Ek, M., Freedman, F., Hamdi, R., Kerstein, A., Kitagawa, H., Lenderink, G., Lewellen, D., Mailhot, J., Mauritsen, T., Perov, V., Schayes, G., Steeneveld, G. J., Svensson, G., Taylor, P., Weng, W., Wunsch, S., and Xu, K.-M.: Single-Column Model Intercomparison for a Stably Stratified Atmospheric Boundary Layer, *Boundary-Layer Meteorology*, 118, 273–303, <https://doi.org/10.1007/s10546-005-3780-1>, publisher: Springer Netherlands, 2005.
- 470



- Donda, J. M. M., van Hooijdonk, I. G. S., Moene, A. F., Jonker, H. J. J., van Heijst, G. J. F., Clercx, H. J. H., and van de Wiel, B. J. H.: Collapse of turbulence in stably stratified channel flow: a transient phenomenon, *Quarterly Journal of the Royal Meteorological Society*, 141, 2137–2147, <https://doi.org/10.1002/qj.2511>, publisher: John Wiley & Sons, Ltd, 2015.
- Foken, T.: 50 Years of the Monin–Obukhov Similarity Theory, *Boundary-Layer Meteorology*, 119, 431–447, <https://doi.org/10.1007/s10546-006-9048-6>, 2006.
- 475 Genthon, C., Town, M. S., Six, D., Favier, V., Argentini, S., and Pellegrini, A.: Meteorological atmospheric boundary layer measurements and ECMWF analyses during summer at Dome C, Antarctica, *Journal of Geophysical Research: Atmospheres*, 115, <https://doi.org/10.1029/2009JD012741>, 2010.
- Genthon, C., Veron, D., Vignon, E., Six, D., Dufresne, J. L., Madeleine, J.-B., Sultan, E., and Forget, F.: Ten years of shielded ventilated atmospheric temperature observation on a 45-m tower at Dome C, East Antarctic plateau, <https://doi.pangaea.de/10.1594/PANGAEA.932512>, status: in review, 2021.
- 480 Hooijdonk, I. G. S. v., Donda, J. M. M., Clercx, H. J. H., Bosveld, F. C., and Wiel, B. J. H. v. d.: Shear Capacity as Prognostic for Nocturnal Boundary Layer Regimes, *Journal of the Atmospheric Sciences*, 72, 1518–1532, <https://doi.org/10.1175/JAS-D-14-0140.1>, publisher: American Meteorological Society Section: *Journal of the Atmospheric Sciences*, 2015.
- 485 Kaiser, A., Faranda, D., Krumscheid, S., Belušić, D., and Vercauteren, N.: Detecting Regime Transitions of the Nocturnal and Polar Near-Surface Temperature Inversion, *Journal of Atmospheric Sciences*, 77, 2921–2940, <https://doi.org/10.1175/JAS-D-19-0287.1>, 2020.
- Kähnert, M.: Advancing the Capabilities of Numerical Weather Prediction - On the Utility of Individual Tendency Output, Doctoral thesis, The University of Bergen, <https://bora.uib.no/bora-xmlui/handle/11250/3030505>, accepted: 2022-11-07T14:32:07Z ISBN: 9788230845776, 2022.
- 490 Lan, C., Liu, H., Katul, G. G., Li, D., and Finn, D.: Turbulence Structures in the Very Stable Boundary Layer Under the Influence of Wind Profile Distortion, *Journal of Geophysical Research: Atmospheres*, 127, e2022JD036565, <https://doi.org/10.1029/2022JD036565>, <https://onlinelibrary.wiley.com/doi/pdf/10.1029/2022JD036565>, 2022.
- Liang, J., Zhang, L., Wang, Y., Cao, X., Zhang, Q., Wang, H., and Zhang, B.: Turbulence regimes and the validity of similarity theory in the stable boundary layer over complex terrain of the Loess Plateau, China, *Journal of Geophysical Research: Atmospheres*, 119, 6009–6021, <https://doi.org/10.1002/2014JD021510>, [eprint: https://onlinelibrary.wiley.com/doi/pdf/10.1002/2014JD021510](https://onlinelibrary.wiley.com/doi/pdf/10.1002/2014JD021510), 2014.
- 495 Mahrt, L.: Nocturnal Boundary-Layer Regimes, *Boundary-Layer Meteorology*, 88, 255–278, <https://doi.org/10.1023/A:1001171313493>, 1998.
- Mahrt, L.: Stably Stratified Atmospheric Boundary Layers, *Annual Review of Fluid Mechanics*, 46, 23–45, <https://doi.org/10.1146/annurev-fluid-010313-141354>, publisher: Annual Reviews, 2014.
- 500 Mahrt, L. and Bou-Zeid, E.: Non-stationary Boundary Layers, *Boundary-Layer Meteorology*, 177, 189–204, <https://doi.org/10.1007/s10546-020-00533-w>, 2020.
- McNider, R. T.: Predictability of the stable atmospheric boundary layer, *Journal of the atmospheric sciences*, 52, 1602–1614, [https://doi.org/10.1175/1520-0469\(1995\)052<1602:POTSAB>2.0.CO;2](https://doi.org/10.1175/1520-0469(1995)052<1602:POTSAB>2.0.CO;2), 1995.
- Pavliotis, G. A.: *Stochastic Processes and Applications*, vol. 60, Springer New York, <https://doi.org/10.1007/978-1-4939-1323-7>, 2014.
- 505 Ramsey, E. and Monahan, A. H.: Empirical Low-Dimensional Dynamics of Atmospheric Stable Boundary Layer Temperature Inversions, *Journal of the Atmospheric Sciences*, 79, 1965–1984, <https://doi.org/10.1175/JAS-D-21-0205.1>, publisher: American Meteorological Society Section: *Journal of the Atmospheric Sciences*, 2022.



- Rößler, A.: Runge–Kutta Methods for the Strong Approximation of Solutions of Stochastic Differential Equations, *SIAM Journal on Numerical Analysis*, 48, 922–952, <https://doi.org/10.1137/09076636X>, publisher: Society for Industrial and Applied Mathematics, 2010.
- 510 Sandu, I., Beljaars, A. C. M., Bechtold, P., Mauritsen, T., and Balsamo, G.: Why is it so difficult to represent stably stratified conditions in numerical weather prediction (NWP) models?, *Journal of Advances in Modeling Earth Systems*, 5, 117–133, <https://doi.org/10.1002/jame.20013>, 2013.
- Sun, J., Mahrt, L., Banta, R. M., and Pichugina, Y. L.: Turbulence Regimes and Turbulence Intermittency in the Stable Boundary Layer during CASES-99, *Journal of the Atmospheric Sciences*, 69, 338–351, <https://doi.org/10.1175/JAS-D-11-082.1>, publisher: American Meteorological Society Section: *Journal of the Atmospheric Sciences*, 2012.
- 515 van de Wiel, B. J. H., Ronda, R. J., Moene, A. F., Bruin, H. A. R. D., and Holtslag, A. a. M.: Intermittent Turbulence and Oscillations in the Stable Boundary Layer over Land. Part I: A Bulk Model, *Journal of the Atmospheric Sciences*, 59, 942–958, [https://doi.org/10.1175/1520-0469\(2002\)059<0942:ITAOIT>2.0.CO;2](https://doi.org/10.1175/1520-0469(2002)059<0942:ITAOIT>2.0.CO;2), 2002.
- van de Wiel, B. J. H., Vignon, E., Baas, P., van Hooijdonk, I. G. S., van der Linden, S. J. A., Antoon van Hooft, J., Bosveld, F. C., de Roode, S. R., Moene, A. F., and Genthon, C.: Regime Transitions in Near-Surface Temperature Inversions: A Conceptual Model, *Journal of Atmospheric Sciences*, 74, 1057–1073, <https://doi.org/10.1175/JAS-D-16-0180.1>, 2017.
- 520 Vercauteren, N., Mahrt, L., and Klein, R.: Investigation of interactions between scales of motion in the stable boundary layer, *Quarterly Journal of the Royal Meteorological Society*, 142, 2424–2433, <https://doi.org/10.1002/qj.2835>, publisher: John Wiley & Sons, Ltd, 2016.
- Vignon, E., van de Wiel, B. J. H., van Hooijdonk, I. G. S., Genthon, C., van der Linden, S. J. A., van Hooft, J. A., Baas, P., Maurel, W., Traullé, O., and Casasanta, G.: Stable boundary-layer regimes at Dome C, Antarctica: observation and analysis, *Quarterly Journal of the Royal Meteorological Society*, 143, 1241–1253, <https://doi.org/10.1002/qj.2998>, 2017.
- 525